Electrodesorption Potentials of Self-Assembled Alkanethiolate Monolayers on Copper Electrodes. An Experimental and Theoretical Study

O. Azzaroni,[†] M. E. Vela,[†] M. Fonticelli,[†] G. Benítez,[†] P. Carro,[‡] B. Blum,[†] and R. C. Salvarezza*,[†]

Instituto de Investigaciones Fisicoquímicas Teóricas y Aplicadas (INIFTA), Universidad Nacional de La Plata-CONICET, Sucursal 4, Casilla de Correo 16, 1900 La Plata, Argentina, and Departamento de Química Física, Universidad de La Laguna, Tenerife, Spain

Electrodesorption potentials for alkanethiolate self-assembled monolayers (SAMs) on polycrystalline Cu and Cu(111) surfaces were determined by using electrochemical techniques combined with Auger electron spectroscopy. For a given alkanethiolate SAM, the electrodesorption potentials from Cu are shifted 0.6 V in the negative direction with respect to those found on Au. Calculations based on density funtional theory for methanethiolate desorption from Cu(111) show that these potential differences reflect differences in the energy for introducing an electron into the alkanethiolate−metal system and also in the energy to break the alkanethiolate S-head−metal bond. On the other hand, the alkanethiolate−alkanethiolate interaction energies at SAMs remain practically independent of the substrate.

1. Introduction

Molecular interactions govern self-assembly processes. The understanding of these interactions is a key point in nanoscience and nanotechnology for the reason that self-assembly has been taken as a preferred route for building complex structures at molecular dimensions. In particular, alkanethiolate self-assembled monolayers (SAMs) on metals have attracted considerable scientific and technological interest because they provide a means to control corrosion, wetting, and wear properties of metal surfaces, they serve to anchor different functional groups used as chemical and biochemical sensors,[1] they are used to fabricate nanodevices for electronics,[2] they are promising candidates for new nanofabrication methods,[3,4] and finally, they are ideal model systems for interface science.[5] Under this focus, alkanethiolate SAMs have been built up on different metal surfaces, such as, Au,[5,6] Ag,[5,6] Cu,[5] Pt,[7] Fe,[8,9] Ni,[10] Pd,[11,12] and alloys,[13,14] with different purposes ranging from corrosion protection to nanofabrication.

The preferred SAM−metal model system has been the alkanethiolate−Au(111) surface because of the high stability of Au in different environments and the easy preparation of clean and ordered Au(111) surfaces. It is well-known that alkanethiolates on Au(111) surfaces form an ordered ($\sqrt{3} \times \sqrt{3}$)$R30°$ lattice[5] and its related $c(4 \times 2)$ superlattice, both in gaseous[15] and in liquid[16] environments. The alkanethiolate molecules in these lattices are chemisorbed on the Au surface by the S-heads, forming a thiolate bond.[17,18] The hydrocarbon chain presents a tilt angle ranging from 20° to 40° with respect to the substrate normal.[19−22] The ($\sqrt{3} \times \sqrt{3}$)$R30°$ lattice exhibits nearest-neighbor distances $d \approx 0.5$ nm,[1] while the $c(4 \times 2)$ lattice exhibits some pairing of the S atoms as revealed by grazing incidence x-ray diffraction (GIXD) data.[5] Scanning tunneling microscopy (STM) measurements have shown $d = 0.45$ nm between the bright and dark spots (interrow distance)

and $d = 0.5$ nm inside the row (intrarow distance) of the $c(4 \times 2)$ superlattices.[16]

In the case of alkanethiolate adsorption on Ag(111), chemisorbed molecules are also bonded by the S head to the Ag surface, although their tilt angle with respect to the substrate normal ranges from 0° to 15°.[23] Previous STM studies have shown that alkanethiolates with large hydrocarbon chains organize on Ag(111) forming a slightly distorted incommensurate ($\sqrt{7} \times \sqrt{7}$)$R19.1°$ hexagonal adlayer with $d = 0.46$ nm,[24] which is expanded with respect to the $d = 0.44$ nm found in the ($\sqrt{7} \times \sqrt{7}$)$R19.1°$ lattice observed for S and short alkanethiols on Ag(111).[25,26] The S-heads of the alkanethiol molecules in the ($\sqrt{7} \times \sqrt{7}$)$R19.1°$ lattice are placed at hollow and top sites.[27] The value $d = 0.46$ nm has also been observed in close-packed bulk alkanes.[6]

Alkanethiols strongly adsorb on Cu(111) promoting a surface layer reconstruction.[28,29] Normal incidence X-ray standing wave (NIXSW) studies have shown that the adsorbate structure is most likely a distortion of the ($\sqrt{3} \times \sqrt{3}$)$R30°$ lattice observed for alkanethiolate adsorption on Au(111).[27] Hexagonal (surface coverage ≈ 0.33) and rectangular (surface coverage ≈ 0.50) surface structures have also been observed by STM.[30,31] Ultrahigh vacuum (UHV) X-ray standing wave (NIXSW) and near-edge X-ray adsorption fine structure (NEXAFS) studies have shown that the alkanethiolate molecules are almost normal to the substrate surface (tilt angle, 12°). For hexanethiolate- and dodecanethiolate-covered Cu(111) (surface coverage 0.33) surface, K-edge surface-extended X-ray absorption fine structure data are consistent with alkanethiol adsorption at fcc-hollow sites.[28] Scanned-energy mode photoelectron diffraction of methanethiolate on unreconstructed Cu(111) has revealed an occupation of 71% of bridge and 29% of fcc sites.[32] During adsorption of methanethiol and other short-chain alkanethiolates on Cu(111)[33] and polycrystalline Cu[34] surfaces at room temperature, a certain amount of S atoms can also be produced.

The nature of the metal surface has been shown to play a key role on the SAM properties, even on metal substrates

* Corresponding author. E-mail: robsalva@infta.unlp.edu.ar.
† Universidad Nacional de La Plata-CONICET.
‡ Universidad de La Laguna.

modified by foreign metals at the monolayer level. Programmed thermal desorption of alkanethiolate SAMs on Cu results in S−C bond scission,[35] in stricking contrast to SAMs on Au, where the organosulfur molecules are completely desorbed, without any C−S bond scission.[5] A Cu monolayer introduced between the Au substrate and the alkanethiolate SAM promotes an enhanced thermal stability of the SAM monolayer in liquid environments.[36,37]

It is clear by now that the self-assembly of these two-dimensional structures implies alkanethiolate−metal, alkanethiolate−alkanethiolate, alkanethiolate−environment, and metal−environment interactions. Previous studies for the alkanethiolate desorption from Au surfaces in hexadecane have reported activation energies that increase 0.84 kJ/mol per methylene unit.[11] Stabilization energies on the order of 1.5 kJ/mol per methylene unit have been proposed from the analysis of different adsorption/desorption data.[39] In the case of electrolyte solutions, reductive electrodesorption curves have been used to estimate these contributions.[40−43] In electrolyte solutions, Au(111)−($\sqrt{3} \times \sqrt{3}$)R30° and c(4 × 2) and Ag(111)−($\sqrt{7} \times \sqrt{7}$)R19.1° alkanethiolate lattices are desorbed in voltammetric peaks according to this reaction

$$(CH_3)(CH_2)_nS\text{-Me} + \text{solvent} + e =$$
$$[(CH_3)(CH_2)_nS^-]_{solv} + Me_{solv} \quad (1)$$
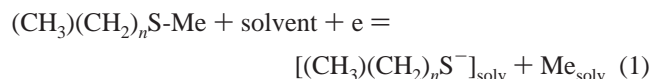
In eq 1, $(CH_3)(CH_2)_nS$−Me stands for the adsorbed alkanethiolate molecule on the Me substrate, $[(CH_3)(CH_2)_nS^-]_{solv}$ for the solvated desorbed alkanethiolate, and Me_{solv} for the solvated substrate. The peak potential (E_p) shifts in the negative potential (E) direction as the number of CH_2 units (n) in the hydrocarbon chain of the alkanethiolate molecules increases. On the basis of the peak potential (E_p) vs n plots, the stabilizing interactions in aqueous 0.1 M NaOH solutions (van der Waals + hydrophobic forces) have been estimated in the 3−4 kJ/mol range per methylene unit, for both Au(111) and Ag(111) substrates.[40,44−46] The magnitude of these interactions decreases to 2 kJ/mol per methylene unit in 0.1 M NaOH methanolic solutions. It has been also shown that for a constant n, the alkanethiolate molecules are desorbed from Ag(111) at more negative potential values than those corresponding for the desorption from Au(111). This difference has tentatively been explained by the smaller work function value or the stronger Lewis acid behavior of Ag with respect to Au.[47]

The information about the electrochemical behavior of alkanethiolate SAMs on Cu(111) in electrolyte solutions is much more limited than that found for SAMs on Ag(111) and Au(111) surfaces. Electrochemical measurements have shown that the best SAM quality on Cu is observed using toluene as a solvent.[48] SAMs on Cu have been proposed as effective barriers of water and ions to be used to protect the metal against corrosion.[49−54] The surface modification treatment should be combined with cathodic protection to eliminate corrosion at SAM defects. Alkanethiolate SAMs on Cu have also been used to modify the adherence properties of metal and alloy electrodeposits to prepare standing-free metallic films.[55,56] There is a major problem, however, for the electrochemical characterization of the alkanethiolate/Cu system arising from the fact that no electrodesorption peaks can be recorded in cathodic polarization curves.[57] This is a result of the hydrogen evolution (HER) reaction taking place, probably at nanoscale SAM defects, before any electrochemical evidence of alkanethiolate electrodesorption can be observed, in contrast to that found for alkanethiolates on Au and Ag. Because of the potential technological applica-

tions of SAMs on Cu, quantitative aspects of the energetics involved in the electrosorption of alkanethiolates on metal surfaces deserves further investigation.

In this paper, we have used electrochemical techniques combined with Auger electron spectroscopy (AES) data to investigate the occurrence of an alkanethiolate SAM electrodesorption process from Cu surfaces and to determine its electrodesorption potential for alkanethiolate SAMs in methanolic solutions. From electrodesorption potentials and DFT calculations, we try to answer relevant questions about these molecular films, such as: Does the S−C bond break during the electrodesorption process as reported in UHV measurements? Is the magnitude of the alkanethiolate−alkanethiolate interaction acting at SAMs on Cu similar to those acting at SAMs formed on Au and Ag? Which are the main energetic contributions that determine the increased stability of alkanethiolate SAM on Cu in electrolyte solutions? Is there any correlation between the surface work function and the SAM electrochemical stability? All of these questions are related to a central problem: the response of molecular films on metal surfaces under an electric field applied to the metal/organic film interface.

Our results show that SAMs on polycrystalline Cu and Cu-(111) are electrodesorbed in a relatively narrow potential range with a well-defined peak potential. Electrodesorption takes place without C−S bond scission. The peak potential is shifted 0.6 and 0.4 V in the negative direction with respect to the peak values found on Au and Ag, respectively. DFT calculations show that these differences arise mainly from differences in the energies required to introduce an electron in the alkanethiolate−Cu system and to break the alkanethiolate S-head−Me bond. In contrast, alkanethiolate−alkanethiolate interaction energies in SAMs prepared on Cu are of the same magnitude as those estimated for SAMs on Au and Ag.

2. Characterization of n-Alkanethiolate Metal Surfaces

2.1. Experimental Procedure. Alkanethiolate monolayers were self-assembled on Cu in toluene solution containing 5 mM alkanethiols (immersion time 2 h at room temperature). Three alkanethiols with different chain length n were used separately: hexanethiol, dodecanethiol, and hexadecanethiol. The presence of electrodesorption peaks were investigated by using a rotating polycrystalline gold ring−polycrystalline copper disk electrode (Figure 1a,b). This method was chosen because first, if alkanethiolate electrodesorption peaks from Cu exist, they are masked by the hydrogen evolution reaction (HER), and second the reductive desorption of the alkanethiolate from a metallic disk results in an anodic peak at a gold ring.[58]

The gold ring−copper disk was first immersed in the alkanethiol-containing solutions for alkanethiolate self-assembly (Figure 1c). Then, the ring−disk electrode was placed in an electrochemical cell containing 0.1 M NaOH + 5% H_2O methanolic solution. The SAM on the gold ring was removed by scanning the ring potential to $E_{ring} = -2.0$ V (Figure 1d) while setting the Cu disk potential at $E_{disk} = -0.8$ V, a potential at which the SAM remains unaltered and no copper oxide formation takes place. Once the gold ring was clean, the copper disk potential was scanned from $E_{disk} = -0.8$ to $E_{disk} = -2.0$ V to electrodesorb the alkanethiolate molecules, while setting $E_{ring} = -0.2$ V to electroadsorb the alkanethiolates removed from the Cu disk. (Figure 1e) The rotation speed of the Cu disk was 5400 rpm, and the collection efficiency of the ring−disk system was 0.25. To test the system, similar experiments were performed by using a gold ring−gold disk electrode.[58] All of the potentials in the text are referred to the saturated calomel electrode (SCE).
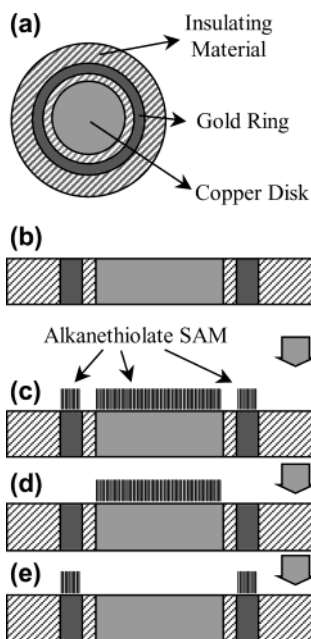
Figure 1. Scheme showing the different steps to determine the alkanethiolate electrodesorption potential range on copper using the rotating ring−disk technique: (a) polycrystalline gold ring−polycrystalline copper disk electrode, top view; (b) polycrystalline gold ring−polycrystalline copper disk electrode, lateral view; (c) polycrystalline gold ring−polycrystalline copper disk electrode after alkanethiolate self-assembly in toluene solutions; (d) alkanethiolate SAM on the copper disk after alkanethiolate electrodesorption from the gold ring; (e) oxidative electroadsorption of alkanethiolate molecules at the Au ring immediately after alkanethiolate electrodesorption from the Cu disk.

In another set of experiments, several clean and dodecanethiol-covered Cu(111) single-crystal samples were prepared, following different steps of the procedures used for the Cu-disk electrode: (i) immersion of the clean Cu(111) crystal in the alkanethiolate solution; (ii) polarization of dodecanethiolate-covered Cu(111) samples for 5 min in a 0.1 M NaOH + 5% H_2O methanolic solution at different constant potentials, followed by a 5 min sonication in cyclohexane to minimize any possible dodecanethiolate readsorption from remaining dodecanethiol micelles. After each treatment, the surface chemical composition of the electrode was analyzed by Auger electron spectroscopy (AES) using a single-pass cylindrical mirror analyzer (CMA, Physical Electronics).

2.2. Electrochemical Results on Polycrystalline Cu. Typical cathodic polarization curves for a dodecanethiolate-covered polycrystalline Cu rotating disk show a constant current region (double layer) followed by a marked cathodic current increase at $E_{disk} = -1.60$ V related to the HER (Figure 2a). No clear features related to alkanethiolate electrodesorption are evident from this curve. On the other hand, the polycrystalline gold ring ($E_{ring} = -0.2$ V) exhibits a clear oxidation peak when the disk potential reaches $E_{disk} = -1.67$ V (Figure 2b). We have made similar runs for hexanethiolate- and hexadecanethiolate-covered Cu disks and recorded similar peaks at the gold ring for $E_{disk} = -1.64$ V (hexanethiolate), and $E_{disk} = -1.75$ V (hexadecanethiolate), that is, the peak potential is *n*-dependent (Figure 3). The peaks at the gold ring can, in principle, be assigned to the oxidative electroadsorption of alkanethiolate molecules collected at the gold ring when alkanethiolate electrodesorption at the copper disk takes place.

To verify this hypothesis, after these runs were complete, the potential of the gold ring was scanned in the negative
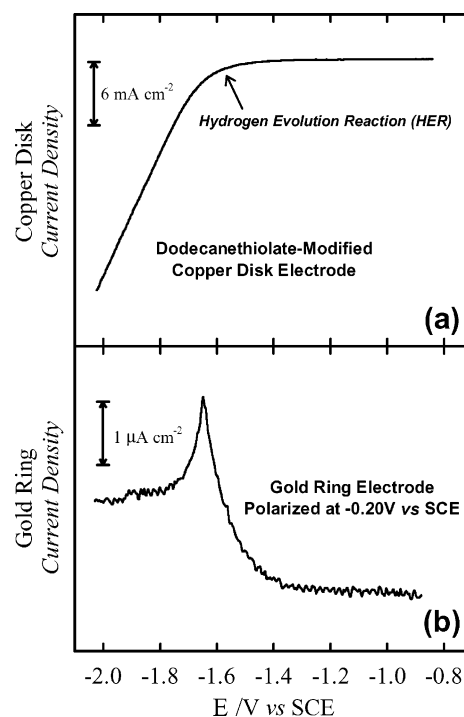

Figure 2. Cathodic polarization curve (a) recorded at 0.05 V/s for a dodecanethiolate-covered polycrystalline copper disk. The onset of the hydrogen evolution reaction is indicated. Panel b shows the anodic current recorded at the polycrystalline gold ring ($E_{ring} = -0.2$ V) during the polarization curve of the dodecanethiolate-covered copper disk shown in panel a.
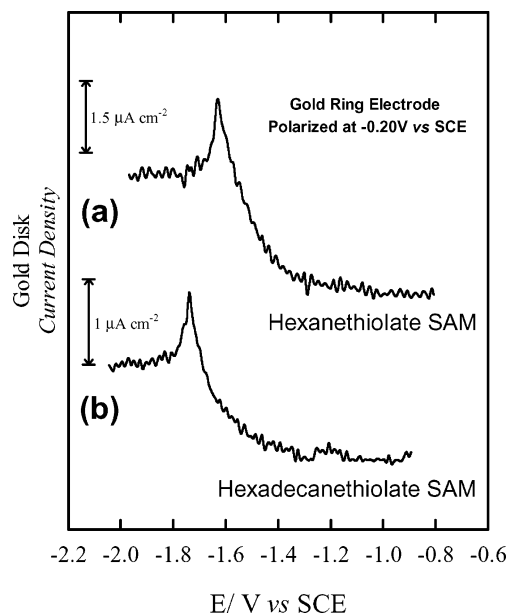

Figure 3. Anodic current at the polycrystalline gold ring ($E_{ring} = -0.2$ V) recorded during the cathodic polarization curve (as shown in Figure 1a) of (a) hexanethiolate-covered and (b) hexadecanethiolate-covered copper disks.

direction. A characteristic alkanethiolate electrodesorption current peak preceding HER was recorded (not shown). The electroreduction peak positions at the gold ring appear at the same *n*-dependent potential values as those expected for the corresponding *n*-alkanethiolate on polycrystalline gold (see Figure 5), confirming the presence of the alkanethiolates. In addition, this indicates that the alkanethiol electrodesorption from the Cu disk takes place without scission of the C−S bond because S electrodesorption from the gold surface takes place
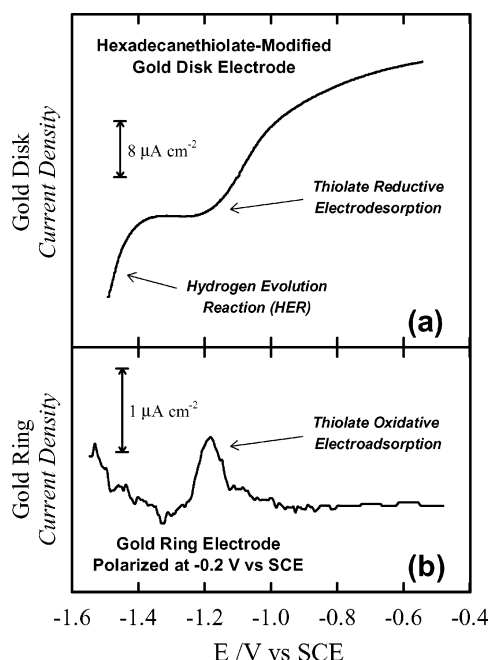
Figure 4. Cathodic polarization curve (a) recorded at 0.05 V/s for a hexadecanethiolate-covered polycrystalline gold disk. Alkanethiolate electrodesorption and the onset of the hydrogen evolution reaction are indicated. Panel b shows the anodic current recorded at the polycrystalline gold ring ($E_{ring} = -0.2$ V) during the polarization curve of the hexadecanethiolate-covered gold disk shown in panel a.
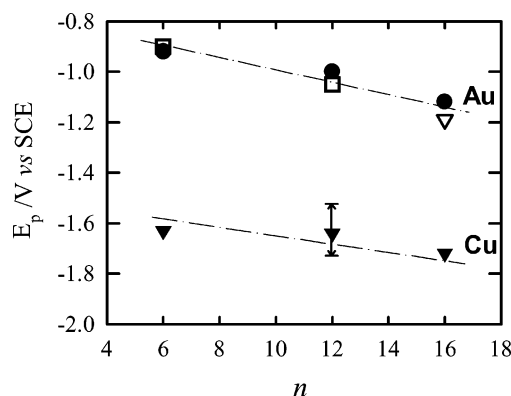

Figure 5. E_p vs n plot for (●) Au(111), determined by cathodic polarization curves (ref 60), (□) polycrystalline Au, measured by cathodic polarization curves (ref 59), (▽) hexadecanethiolate-covered polycrystalline ring, determined by cathodic polarization curves after oxidative electroadsorption of hexadecanethiolate produced by the electroreduction of the organic adsorbates from the Cu disks, and (▼) polycrystalline Cu determined by the rotating ring−disk technique. The bar for $n = 12$ indicates the potential window at which dodecanethiolates desorb from the Cu(111) surface determined by combined electrochemical polarization and AES.

at a single well-defined peak that obviously does not change with n.[44]

To support the idea that the peak potentials derived from the ring current can be taken as "true peak potentials" for alkanethiolate electrodesorption from the Cu disk, similar cathodic polarization curves were recorded using a gold ring/hexadecanethiolate-covered gold disk (Figure 4). In this case, the peak potential for alkanethiolate electrodesorption from the gold disk (Figure 4a) is in good agreement with that derived from the gold ring current signal (Figure 4b). Therefore, it can be concluded that, for our systems, alkanethiolate electrodesorption from the disk can be simultaneously detected at the ring. Note, however, that these ring−disk measurements give reliable values for the electrodesorption potential but cannot be used for a accurate quantitative estimation of the amount of electrodesorbed species at the disk. In fact, unstable alkanethiolate micelles are formed on the electrode neighboring as an intermediate product of the electrodesorption process. These micelles slowly decay with time leading to alkanethiolate molecules in the electrolyte.

It should be noted that the onset of alkanethiolate electrodesorption in Figure 2b takes place at −1.35 V, a value for which the current related to HER is negligible (Figure 2a) although the reversible potential for the HER in the working solution is −1.03 V. This means that the alkanethiolate SAMs on Cu have high blocking properties with a small amount of pinholes, as already concluded from the behavior of SAM-covered Cu electrodes against corrosion.[53] The analysis of Figure 2 also reveals that alkanethiolate desorption takes place simultaneously with HER, that is, hydrogen evolution takes place immediately as bare Cu domains are produced.

The E_p values derived from this technique for different alkanethiolate-covered Cu and Au disks are shown in Figure 5. In this plot, we have also included E_p values for different SAMs on Au(111) and polycrystalline Au in methanolic and ethanolic solutions.[59] Two main conclusions can be derived from this plot: (i) E_p values derived from polycrystalline Au and Au(111)

are in good agreement, so in principle, no marked differences should be expected between Cu(111) and polycrystalline Cu substrates; (ii) E_p values for hexadecanethiolate electrodesorption from Au derived from the rotating ring−disk technique agree very well with that measured by voltammetry in a previous paper,[60] thus supporting the conclusion derived from the analysis of Figure 4.

2.3. AES Data on Cu(111) Surfaces. The results described above were obtained using a rotating polycrystalline Au ring−polycrystalline Cu disk electrode. On the basis of this information, we have studied the electrodesorption of dodecanethiolate-covered Cu(111) combining electrochemical measurements and AES. Note that in situ STM is not suitable for the study of alkanethiolate electrodesorption from Cu surfaces because of the large faradaic currents related to HER in the potential range of alkanethiolate desorption (Figure 2). The formation of hydrogen bubbles is another source of instability that also precludes the use of in situ scanning probe microscopies (STM; atomic force microscopy, AFM) to obtain information about the electrodesorption process. This is not the case for alkanethiolate electrodesorption from Au surfaces where in situ scanning probe microscopy (SPM) techniques have been widely used.[56]

In Figure 6, we show a broad Auger electron spectrum of the dodecanethiolate-covered Cu(111) surface after the self-assembly process by immersion. Cu (MVV), S (LLV), C (KLL), and Cu (LMM) transitions are clearly resolved at 60, 152, 271, and 700−900 eV, respectively. Only trace amounts of O (KLL, 503 eV) are present, that is, no significant amounts of copper oxides have been formed during the self-assembly process.

Figure 7 shows the Cu (MVV) and S (LLV) energy region for clean (Figure 7a) and dodecanethiolate-covered (Figure 7b−d) Cu(111) surfaces. The presence of the organic molecule after the self-assembly process (Figure 7b) is clearly revealed by the S signal at 152 eV. From the Cu (MVV)/S peak-to-peak signal ratio, the surface coverage of dodecanethiolate molecules self-assembled on the Cu(111) electrode results in ∼0.4 ± 0.1 ML, a value expected for mixed hexagonal and square lattices reported for alkanethiolate adsorption on Cu(111).[30,31] A similar surface coverage (within the experimental error) is observed for the polycrystalline Cu electrodes, although in this case the surface structure is not known.
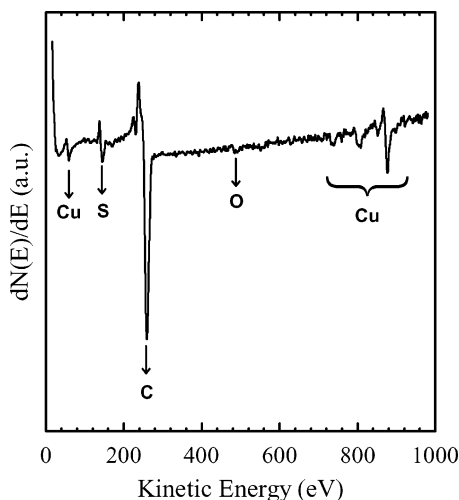
Figure 6. Broad AES spectra for a dodecanethiolate-covered Cu(111) single-crystal surface. Relevant peaks are labeled.
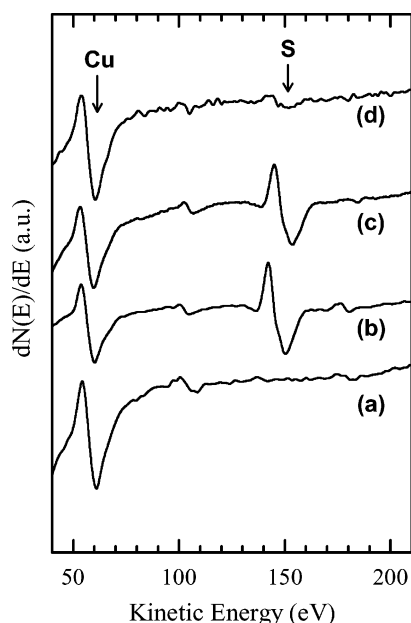

Figure 7. AES spectra corresponding to (a) clean Cu(111), (b) dodecanethiolate-covered Cu(111), (c) dodecanethiolate-covered Cu-(111) after 5 min at $E_{disk} = -1.5$ V in the methanolic solution, and (d) dodecanethiolate-covered Cu(111) after 5 min at $E_{disk} = -1.7$ V in the methanolic solution.

Figure 7c,d shows the AES spectra obtained for dodecanethiolate-covered Cu(111) electrodes after polarization at $E_{disk} = -1.50$ V (Figure 7c) and $E_{disk} = -1.70$ V (Figure 7d). The spectrum taken for $E_{disk} = -1.5$ V (Figure 7c) in the methanolic solution is similar to the one recorded before immersion in the ring−disk electrochemical cell (Figure 7b), suggesting that the surface coverage remains unaltered by polarization at this potential value in the electrolyte. On the other hand, the marked decrease in the S signal for the sample held at $E_{disk} = -1.70$ V (Figure 7d) indicates that dodecanethiolate electrodesorption from the Cu(111) surface takes place at this potential. Therefore, we conclude that the peak potential for dodecanethiolate electrodesorption from Cu(111) should be in the $-1.70 < E_p < -1.50$ V region, in good agreement with the ring−disk data for polycrystalline Cu ($E_p = -1.67$ V).

In summary, our combined electrochemical and AES results show that the E_p value for the electrodesorption of an *n*-alkanethiolate from the Cu surface is shifted by about 0.6 V in the negative direction with respect to the corresponding E_p value

from a Au surface (Figure 5). That is, SAMs on Cu are considerably more stable than those formed on Au surfaces. This explains why Ni and NiCoFe alloys have been successfully deposited on dodecanethiolate-covered Cu from aqueous solutions at potentials as negative as −1.2 V[55] with no significant SAM damage. In this case, the presence of the SAM at the Cu surface has been verified by the low adherence of the metal deposits and contact angle measurements after the NiCoFe electrodeposit detachment. On the other hand, similar experiments on dodecanethiolate-covered Au result in dodecanethiolate elecrodesorption and micelle formation before Ni electrodeposition.[56] These marked differences in E_p values and SAM stability originate from different energetic contributions on either substrate. To identify the differences in energy that produce the marked stability of SAMs on Cu in electrolyte solutions, with respect to gold, we have estimated the adsorption energy of alkanethiolate molecules on Cu(111) surfaces by using DFT calculations.

3. Quantum Density Functional Theory (DFT) Calculations

3.1. Method. Several studies address the adsorption of neutral alkanethiol species on Au(111),[61−65] Ag(111),[61] and Cu(111).[64] However, as was noted in the Introduction (eq 1), the reductive electrodesorption process in aqueous media results in alkanethiolate anion formation. Adsorption energies of negatively charged anion methanethiolate (CH_3S^-) have only been estimated for Au(111) and Ag(111) surfaces.[60] Following this calculation procedure, we estimate the adsorption energies of methanethiolate on different high-symmetry Cu(111) sites and compare these values with those obtained for Ag(111) and Au(111) surfaces, as described below.

DFT calculations are based on the three-parameter hybrid method proposed by Becke, associated with the gradient-corrected correlation functional of Lee, Yang, and Parr, B3LYP.[66] The methanethiolate anion was oriented with the sulfur atom oriented toward the metal (Me) surface at a certain distance over the selected surface site. The S−Me distance (d) and the α angle defined between the C−S bond and the substrate normal were optimized while holding the rest of the anion geometry fixed throughout the calculations at the optimized values of the isolated anion.

The metal atoms have been described with 11 electrons, whereas the remainder of the atomic electron density was replaced by relativistic effective core potential (ECP) from Hay and Wadt, LANL1MB.[67] The $n d^{10} (n+1) s^1$ valence shells, $n = 3$ for Cu, $n = 4$ for Ag, and $n = 5$ for Au, were treated explicitly with the basis set LANL1MB. S, C, and H atoms are described with the standard 6-31G(d) basis set,[68] which is split valence plus polarization quality. In all cases, the electronic state considered is taken as the lowest-energy closed-shell configuration. The theoretical calculations were performed with the electronic structure software Gaussian 98.[69] We have also calculated the charge remaining in the S atom after methanethiolate adsorption by using Mulliken populations. These are used as a qualitative tool because of their well-known limitations.

The cluster model used to represent the metal surface was built with 10 atoms distributed seven in the top layer and three in the second layer (Figure 8). The metal−metal distance was maintained fixed to the bulk value 0.2556, 0.2884, and 0.2889 nm for Cu, Ag, and Au, respectively. We have studied four surface sites: hollow hcp, hollow fcc, bridge, and top (Figure 9) for Cu and Ag. Note that hcp and fcc sites involve tetrahedral and octahedral coordination geometries, respectively. In the case
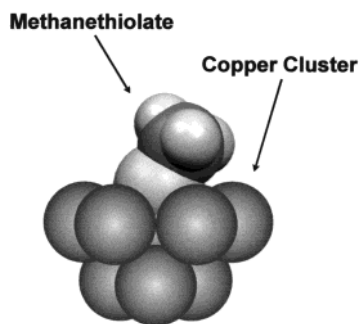
Figure 8. Three-dimensional scheme (lateral view) showing the methanethiolate molecule on the Cu(111) cluster used for DFT calculations.
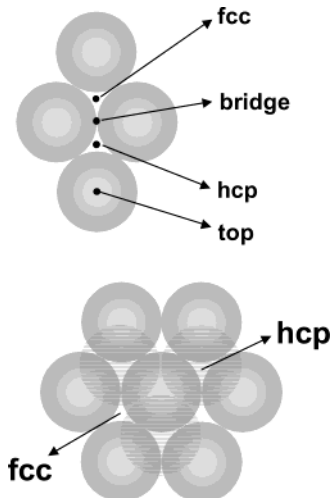

Figure 9. Scheme (top view) showing the different sites studied for methanethiolate adsorption on the Cu(111) surface.

of the Au(111) surface our calculations were also extended to the hcp-bridge and fcc-bridge sites. The methanethiolate anion was placed with the sulfur atom oriented toward the metal (Me) surface at a certain distance over the selected surface site. The S–Me distance (d) and the angle α defined between the C–S bond and the substrate normal were optimized while holding the rest of the anion geometry fixed throughout the calculations at the optimized values of the isolated anion.

The methanethiolate adsorption energy, E_{ads}, has been defined as

$$E_{ads} = E[Me_{10}SCH_3]^- - [E[Me_{10}] + E[SCH_3^-]] \quad (2)$$

where $E[Me_{10}SCH_3]^-$ is the total energy of $[Me_{10}SCH_3]^-$ with the parameters d and α optimized, $E[Me_{10}]$ is the energy for the 10-atom metal cluster, and $E[SCH_3^-]$ is the energy of methanethiolate anion.

3.2. Numerical Results. Results obtained for the methanethiolate anion adsorption on Cu(111) surfaces are summarized in Table 1 and compared to those previously reported[60] for methanethiolate adsorption on Au(111) and Ag(111). S–Me bond lengths (d)[10] and α angles are similar to those calculated for methanethiol adsorption on Cu(111).[64] The magnitude of the E_{ads} value for methanethiolate adsorption on Cu(111) substrate sites agrees with that recently reported[64,70] and with the values estimated for negatively single-charged anions adsorbed on (111) faces. The E_{ads} values differ no more than 40 kJ mol^{-1} for the different Cu(111) sites. Note that the adsorption energies at hollow hcp, hollow fcc, and bridge differ by less than 10 kJ mol^{-1}. In the case of E_{ads} for the Au(111)
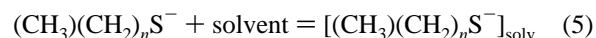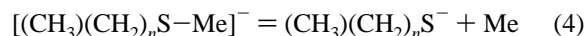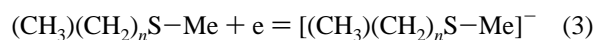
TABLE 1: Desorption Energy ($-E_{ads}$), S–Me Bond Length (d), α Value, Charge on the S Atom, Energy of the Highest Occupied Molecular Orbital (ϵ_{HOMO}), and Energy Difference between Charged and Neutral Species (ΔE_{c-n}) for Methanethiolate Adsorbed on the Different Metal Sites

metal	site	d, nm	α, deg	$-E_{ads}$, kJ mol^{-1}	charge on the S atom	$-\epsilon_{HOMO}$, eV	$-\Delta E_{c-n}$, kJ mol^{-1}
Au(111)	hcp	0.227	23.8	246	−0.13	1.18	241.24
	fcc	0.232	58.5	255	−0.15	1.08	245.18
	top	0.260	73.5	209	−0.21	1.23	
	hcp-bridge	0.233	50.5	250	−0.16	1.19	242.6
	fcc-bridge	0.236	30.0	249	−0.18	1.22	244.12
	bridge	0.234	24.9	226	−0.18	1.20	
Ag(111)	hcp	0.226	33.3	223	−0.28	0.53	170.62
	fcc	0.230	1.96	212	−0.28	0.45	158.55
	top	0.263	68.1	180	−0.31	0.54	183.75
	bridge	0.234	34.8	194	−0.29	0.54	
Cu(111)	hcp	0.208	39.0	238	−0.20	0.36	158.21
	fcc	0.207	22.1	228	−0.25	0.26	155.08
	top	0.243	67.3	198	−0.25	0.41	169.26
	bridge	0.217	55	234	−0.22	0.34	162.56

surface similar values were obtained for the fcc, hcp, hcp-brige, and fcc-bridge. The E_{ads} for the fcc site is slightly higher than that recently reported using the same procedure.[60] On average, E_{ads} increases in the following sequence, Ag(111) < Cu(111) < Au(111). Results also show that the S atoms in the C–S–Cu and C–S–Ag bonds have a greater negative charge than that of the S atom in the C–S–Au bond in agreement with x-ray photoelectron spectroscopy (XPS) data.[71]

Reaction 1 involves a charge transfer to a neutral alkanethiolate–Me species. The energetics of this step can be estimated from the energy (ϵ_{HOMO}) of the highest occupied molecular orbital (HOMO) rather than considering work function values as already suggested.[47] Note that ϵ_{HOMO}, which can be estimated directly from the DFT calculations, can be considered as a true ionization potential.[72] Results show that the energy required to introduce an electron into the negatively charged alkanethiolate–metal cluster increases in the following sequence: Cu(111) < Ag(111) < Au(111), as concluded from the analysis of the ϵ_{HOMO} values shown in Table 1. Finally we have also calculated the energetics of the charge-transfer process by using the energy difference (ΔE_{c-n}) between $[Me_{10}SCH_3]^-$ and $[Me_{10}SCH_3]$ species for the most probable adsorption sites of the Cu(111), Ag(111), and Au(111) surfaces. Results show the same trend that is derived from the ϵ_{HOMO} values (Table 1).

3.3. Comparative Stability of *n*-Alkanethiolates on Different Metal Substrates. The reductive desorption process of an alkanethiolate molecule from a metal substrate (Me) in a solvent (solv) can be described by the following reaction steps:[60]

$$(CH_3)(CH_2)_nS-Me + e = [(CH_3)(CH_2)_nS-Me]^- \quad (3)$$

$$[(CH_3)(CH_2)_nS-Me]^- = (CH_3)(CH_2)_nS^- + Me \quad (4)$$

$$(CH_3)(CH_2)_nS^- + solvent = [(CH_3)(CH_2)_nS^-]_{solv} \quad (5)$$

$$Me + solvent = Me_{solv} \quad (6)$$

The energy barrier to desorb an alkanethiolate molecule from the metal surface should involve alkanethiolate–substrate (E_{A-Me}), alkanethiolate–alkanethiolate (E_{A-A}), alkanethiolate–solvent (E_{A-solv}), and substrate–solvent ($E_{Me-solv}$) interaction energies.[12,14] The energy involved in step 3 (E_{ct}) is related to the energy needed to introduce an electron into the alkanethiolate–metal system.[73] Step 4 involves the desorption energy

(E_{des}); $E_{des} = -E_{ads}$, which is n-independent as already discussed[1]. Therefore, E_{A-Me} contains both E_{ct} and E_{des}. Step 4 also involves the breaking of hydrocarbon chain−hydrocarbon chain interactions (E_{A-A}). Finally, steps 5 and 6 involve E_{A-solv} and $E_{Me-solv}$, respectively. The total energy (E_{ed}) involved in the electrodesorption process is

$$E_{ed} = E_{des} + E_{A-solv} + E_{A-A} + E_{Me-solv} + E_{ct} \quad (7)$$

For $n = 0$, the n-dependent terms E_{A-solv} and E_{A-A} cancel so that eq 7 becomes

$$E_{ed}^{n=0} = E_{ct} + E_{des} + E_{Me-solv} \quad (8)$$

ϵ_{HOMO} values are good estimates for E_{ct}[74] and can be taken as effective ionization potentials[72]. The copper−methanol interaction energy value, $E_{Me-solv} = -35$ kJ/mol, is close to that reported for methanol adsorption on Au ($E_{Me-solv} = -35.15$ kJ mol^{-1}) but smaller than that reported on Ag ($E_{Me-solv} = -43.938$ kJ mol^{-1})[75]. Even though we used a mixture of 95% methanol and 5% water as electrolyte, rather than pure methanol, the adsorption energy of methanol is greater than the adsorption energy of water on these surfaces. Therefore, the use of the adsorption energy corresponding to methanol seems to be justified[76]. To calculate E_{des} for the alkanethiolate−copper(111) system, we have used $E_{des} = yE_{des,fcc} + xE_{des,bridge}$ (Table 1) where $x = 0.21$ and $y = 0.79$ according to the site occupancy reported for methanethiolate adsorption on copper[32]. In the case of alkanethiolate−silver(111) we have used $E_{des} = (E_{des,top} + E_{des,hcp} + E_{des,fcc})/3$ because the surface structure consists of a $(\sqrt{7} \times \sqrt{7})R19.1°$ alkanethiolate lattice involving these sites[26]. Finally, for the alkanethiolate−gold(111), we have considered $E_{des} = (E_{des,hcp} + E_{des,bridge-hcp} + E_{des,bridge-fcc} + E_{des,fcc})/4 = 250$ kJ mol^{-1} because the adsorption sites for the $(\sqrt{3} \times \sqrt{3})$-$R30°$ and $c(4 \times 2)$ lattices on Au(111) are not well established[61,77]. We have used the same procedure to estimate the ϵ_{HOMO} values involved in the first electrodesorption step for Cu, Ag, and Au. Thus, by introducing ϵ_{HOMO}, E_{des}, and $E_{Me-solv}$, we obtain

Cu(111), $E_{ed}^{n=0} = -30.87$ kJ mol^{-1} + 232.26 kJ mol^{-1} +

$\qquad (-35.00)$ kJ mol^{-1} = 166.39 kJ mol^{-1}

Au(111), $E_{ed}^{n=0} = -116.73$ kJ mol^{-1} + 250 kJ mol^{-1} +

$\qquad (-35.15)$ kJ mol^{-1} = 98.08 kJ mol^{-1}

Ag(111), $E_{ed}^{n=0} = -49.20$ kJ mol^{-1} + 205 kJ mol^{-1} +

$\qquad (-43.93)$ kJ mol^{-1} = 111.87 kJ mol^{-1}

which means that $\Delta E_{ed}^{n=0}(Ag(111)-Au(111)) = 14$ kJ mol^{-1} and $\Delta E_{ed}^{n=0}(Cu(111)-Au(111)) = 68$ kJ mol^{-1}. When a one-electron charge transfer (eq 1) is considered, the estimated difference in the peak potential results in $\Delta E_p^{n=0}(Ag(111)-Au(111)) = 0.15$ V and $\Delta E_p^{n=0}(Cu(111)-Au(111)) = 0.70$ V. On the other hand, using ΔE_{c-n} (Table 1) instead of ϵ_{HOMO} values and following the same procedure described above for E_{des} and ϵ_{HOMO}, we obtain $\Delta E_p^{n=0}(Ag(111)-Au(111)) = 0.19$ V and $\Delta E_p^{n=0}(Cu(111)-Au(111)) = 0.65$ V.

In principle, electrochemical potentials relate to free energies rather than energies in the enthalpy sense. However, the entropy changes involved in going from ordered alkanethiolate lattices on the Ag(111), Au(111), or Cu(111) surfaces to solvated alkanethiolates in the methanolic solution should be similar. Thus, entropy contributions are canceled when considering free

energy differences in the reductive electrodesoption taking place on these metals.

Another interesting conclusion that can be derived from this analysis is that there is no correlation between substrate work function, $\phi_{Ag} = 4.45$ eV, $\phi_{Cu} = 4.94$ eV, $\phi_{Au} = 5.29$ eV,[78,79] and electrodesorption potentials. The electrodesorption potential shift from one metal electrode to another mainly results from a balance between the alkanethiolate adsortion energy and the energy to introduce an electron into the alkanethiolate−metal system, which is reflected in ϵ_{HOMO} and ΔE_{c-n} values. Note that in our systems the energetic contribution concerning differences in the metal electrode solvation is not significant in the determination of the E_p shift.

For the reductive electrodesorption of different alkanethiolates from the substrate Me in a given solvent, the terms E_{des}, ϵ_{HOMO}, and $E_{Me-solv}$ cancel. Therefore, the energy difference ($\Delta E_{edMe}^{\delta n} = E_{Me}^{n_2} - E_{Me}^{n_1}$) for this process is given only by the n-dependent terms

$$\Delta E_{edMe}^{\delta n} = \Delta E_{A-solv} + \Delta E_{A-A} \quad (9)$$

Note that we can neglect the n-dependent long-range adsorbate−substrate interactions at physisorbed micelles[80] because they are not formed in methanolic solutions[81]. Therefore, for a given substrate, the shift in the E_p value with n should reflect mainly ΔE_{A-solv} and ΔE_{A-A} contributions.

When χ is defined as the increment in electrodesorption energy per methylene unit and the corresponding slope for E_p vs n plot (Figure 5) is considered, χ results in 1.5 kJ mol^{-1} per methylene unit, close to the 1.8 kJ mol^{-1} per methylene unit reported for alkanethiolate electrodesoprtion from Au(111) and Ag(111) surfaces in the same electrolyte. These values are smaller than $\chi = 3-4$ kJ mol^{-1} per methylene unit obtained in aqueous solutions for SAMs on Ag(111) and Au(111) because of the alkanethiolate−methanol interaction energy that favors electrodesorption. The fact that the χ value for Cu, Au, and Ag in the same electrolyte is similar supports the validity of eq 9, that is, χ depends mainly on the n-dependent terms. Note that, on average, considering the interaction energies resulting from the alkanethiolate two-dimensional phases self-assembled on the Cu(111), Ag(111), and Au(111) surfaces, the stabilizing term contributed from the molecular packing should be of the same magnitude. This allows us to draw stability diagrams for alkanethiolate SAMs on Cu(111), Ag(111), and Au(111) in methanolic solutions (Figure 10). In the same plot, we have included the experimental E_p values for Au(111) and Ag(111) from references,[60] and the experimental E_p data obtained in this work using the rotating ring−disk electrodes. For each metal, we have included the calculated plots using ϵ_{HOMO} and ΔE_{c-n}. Estimated magnitudes from quantum chemical calculations are in good agreement with those obtained by using combined electrochemical and surface-sensitive techniques.

Conclusions

We have determined the existence of defined electrodesorption potentials for alkanethiolate SAMs on Cu with no rupture of the C−S bond by using specially adapted electrochemical techniques combined with AES. For a given alkanethiolate SAM, the electrodesorption peak potentials on polycrystalline Cu and Cu(111) surfaces are very similar to each other and are shifted 0.6 and 0.4 V in the negative direction with respect to those found on Au and Ag, respectively. DFT calculations for methanethiolate desorption from Cu(111) show that these potential shifts reflect differences in the energy to introduce an
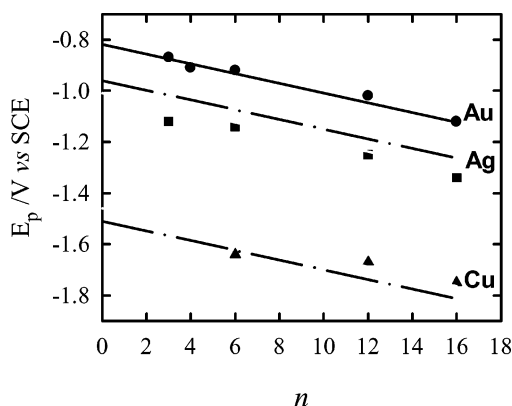
Figure 10. E_p vs n plots for alkanethiolate electrodesorption from Au, Ag, and Cu electrodes in alkaline methanolic solutions. The solid line corresponds to the linear regression derived from experimental data obtained on Au electrodes. The gray solid lines correspond to the theoretical E_p vs n plots for Ag and Cu electrodes (as indicated) obtained by shifting the Au plot in accordance to the energetic calculation depicted by eq 8 and detailed in the text and considering the term E_{c-n} as the energetic contribution of the charge-transfer process. The dashed lines correspond to the theoretical E_p vs n plots for Ag and Cu electrodes obtained by the same procedure described above but considering ϵ_{HOMO} as the energetic contribution of the charge-transfer process. Experimental points are also indicated: (●) Au (from ref 60); (■) Ag (from ref 60); (▲) Cu.

electron into the alkanethiolate−copper system and in the energy for breaking the alkanethiolate S-head−Me bond. On the other hand, the alkanethiolate−alkanethiolate interaction energies at SAMs remain essentially independent of the substrate.

References and Notes

(1) Finklea, H. O. In *Encyclopedia of Analytical Chemistry: Applications, Theory and Instrumentation*; Meyers, R., Ed.; John Wiley & Sons: Chichester, U.K., 2000.

(2) Haag, R.; Rampi, A. M.; Holmlin, R. E.; Whitesides, G. M. *J. Am. Chem. Soc.* **1999**, *121*, 7895.

(3) Xia, Y.; Rogers, J. A.; Paul, K. E.; Whitesides, G. M. *Chem. Rev.* **1999**, *99*, 1823.

(4) Schilardi, P. L.; Azzaroni, O.; Salvarezza, R. C. *Langmuir* **2001**, *17*, 2747.

(5) Schreiber, F. *Prog. Surf. Sci.* **2000**, *65*, 151 and references therein.

(6) Ulman, A. *Chem. Rev.* **1996**, *96*, 1533.

(7) Dreesen, L.; Humbert, C.; Celebi, M.; Lemaire, J. J.; Mani, A. A.; Thiry, P. A.; Peremans, A. *Appl. Phys. B* **2002**, *74*, 621.

(8) Volmer, M.; Czodrowski, B.; Stratmann, M. *Ber. Bunsen-Ges. Phys. Chem.* **1988**, *92*, 1335.

(9) Volmer-Uebing, M.; Stratmann, M. *Appl. Surf. Sci.* **1992**, *55*, 19.

(10) Mekhalif, Z.; Delhalle, J.; Pireaux, J.-J.; Noël, S.; Houzé, F.; Boyer, L. *Surf. Coat. Technol.* **1998**, *100−101*, 463.

(11) Carvalho, A.; Geissler, M.; Schmid, H.; Michel, B.; Delamarche, E. *Langmuir* **2002**, *18*, 2406.

(12) Love, J. C.; Wolfe, D. B.; Chabinyc, M. L.; Paul, K. E.; Whitesides, G. M. *J. Am. Chem. Soc.* **2002**, *124*, 1576.

(13) Pirlot, C.; Delhalle, J.; Pireaux, J. J.; Mekhalif, Z. *Surf. Coat. Technol.* **2001**, *138*, 166.

(14) Mekhalif, Z.; Lazarescu, A.; Hevesi, L.; Pireaux, J.-J.; Delhalle, J. *J. Mater. Chem.* **1998**, *8*, 545.

(15) Anselmetti, D.; Baratoff, A.; Guntherodt, H. J.; Delamarche, E.; Michel, B.; Gerber, Ch.; Kang, H.; Wolf, H.; Ringsdorf, H. *Europhys. Lett.* **1994**, *27*, 365.

(16) Terán, F. T.; Vela, M. E.; Salvarezza, R. C.; Arvia, A. J. *J. Chem. Phys.* **1998**, *109*, 5703.

(17) Zhong, C.-J.; Brush, R. C.; Anderegg, J.; Porter, M. D. *Langmuir* **1999**, *15*, 518.

(18) Vericat, C.; Vela, M. E.; Andreasen, G.; Salvarezza, R. C.; Vázquez, L.; Martín-Gago, J. A. *Langmuir* **2001**, *17*, 4919.

(19) Porter, M. D.; Bright, T. B.; Allara, D. L.; Chidsey, C. E. D. *J. Am. Chem. Soc.* **1987**, *109*, 3559.

(20) Nuzzo, R. G.; Dubois, L. H.; Allara, D. L. *J. Am. Chem. Soc.* **1990**, *112*, 558.

(21) Bryant, M. A.; Pemberton, J. E. *J. Am. Chem. Soc.* **1991**, *113*, 8284.

(22) Hähner, G.; Wöll, C.; Buck, M.; Grunze, M. *Langmuir* **1993**, *9*, 1955.

(23) Nemetz, A.; Fischer, T.; Ulman, A.; Knoll, W. *J. Chem. Phys.* **1993**, *98*, 5912.

(24) Dhirani, K. S.; Hines, A.; Fischer, A. J.; Ismail, O.; Guyot-Sionnest, P. *Langmuir* **1995**, *11*, 2609.

(25) Aloisi, G. D.; Cavallini, M.; Innocenti, M.; Foresti, M. L.; Pezzatini, G.; Guidelli, R. *J. Phys. Chem. B* **1997**, *101,* 4774.

(26) Heinz, R.; Rabe, J. P. *Langmuir* **1995**, *11*, 506.

(27) Rieley, H.; Kendall, G. K.; Jones, R. G.; Woodruff, D. P. *Langmuir* **1999**, *15*, 8856.

(28) Imanishi, A.; Isawa, K.; Matsui, F.; Tsuduki, T.; Yokoyama, T.; Kondoh, H.; Kitajima, Y.; Ohta, T. *Surf. Sci.* **1998**, *407*, 282.

(29) Rieley, H.; Kendall, G. K.; Chan, A.; Jones, R. G.; Lüdecke, J.; Woodruff, D. P.; Cowie, B. C. C. *Surf. Sci.* **1997**, *392*, 143.

(30) Driver, S. M.; Woodruff, D. P. *Langmuir* **2000**, *16*, 6693.

(31) Driver, S. M.; Woodruff, D. P. *Surf. Sci.* **2000**, *457*, 11.

(32) Toomes, R. L.; Polcik, M.; Kittel, M.; Hoeft, J.-T.; Sayago, D. I.; Pascal, M.; Lamont, C. L. A.; Robinson, J.; Woodruff, D. P. *Surf. Sci.* **2002**, *513*, 437.

(33) Jackson, G. J.; Woodruff, D. P.; Jones, R. G.; Singh, N. K.; Chan, A. S. Y.; Cowie, B. C. C.; Formoso, V. *Phys. Rev. Lett.* **2000**, *84*, 119.

(34) Laibinis, P. E.; Whitesides, G. M.; Allara, D. L.; Tao, Y.-T.; Parikh, A. N.; Nuzzo, R. G., *J. Am. Chem. Soc.* **1991**, *113*, 7152.

(35) Loepp, G.; Vollmer, S.; Witte, G.; Wöll, Ch. *Langmuir* **1999**, *15*, 3767.

(36) Jennings, G. K.; Laibinis, P. E. *Langmuir* **1996**, *12*, 6173.

(37) Jennings, G. K.; Laibinis, P. E. *J. Am. Chem. Soc.* **1997**, *119*, 5208.

(38) Bain, C. D.; Troughton, E. B.; Tao, Y.; Evall, J.; Whitesides, G. M.; Nuzzo, R. G. *J. Am. Chem. Soc.* **1989**, *111*, 321.

(39) Schwartz, D. *Annu. Rev. Phys. Chem.* **2001**, *52*, 107.

(40) Widrig, C. A.; Chung, C.; Porter, M. D. *J. Electroanal. Chem.* **1991**, *310*, 335.

(41) Walczak, M.; Alves, C. A.; Lamp, B. D.; Porter, M. D. *J. Electroanal. Chem.* **1995**, *396*, 103.

(42) Zhong, C.-J.; Porter, M. D. *J. Electroanal. Chem.* **1997**, *425*, 147.

(43) Walczak, M. M.; Chung, C.; Stole, S. M.; Widrig, C. A.; Porter, M. D. *J. Am. Chem. Soc.* **1991**, *113*, 2370.

(44) Vela, M. E.; Martin, H.; Vericat, C.; Andreasen, G.; Hernández-Creus, A.; Salvarezza, R. C. *J. Phys. Chem. B* **2000**, *104*, 11878.

(45) Hatchett, D. W.; Stevenson, K. J.; Lacy, W. B.; Harris, J. M.; White, H. S. *J. Am. Chem. Soc.* **1997** *119*, 6596.

(46) Hatchett D. W.; Uibel, R. H.; Stevenson, K. J.; Harris, J. M.; White, H. S. *J. Am. Chem. Soc.* **1998**, *120*, 1062.

(47) Mohtat, N.; Byloos, M.; Soucy, M.; Morin, S.; Morin, M. *J. Electroanal. Chem.* **2000**, *484*, 120.

(48) Ron, H.; Cohen, H.; Matlis, S.; Rappaport, M.; Rubinstein, I. *J. Phys. Chem. B* **1998**, *102*, 9861.

(49) Yamamoto, Y.; Nishihara, H.; Aramaki, K. *J. Electrochem. Soc.* **1998**, *140*, 436.

(50) Jennings, G. K.; Munro, J. C.; Yong, T.-H.; Laibinis, P. E. *Langmuir* **1998**, *14*, 6130.

(51) Feng, Y.; Teo, W.-K.; Siow, K.-S.; Gao, Z.; Tan, K.-L.; Hsieh, A.-K. *J. Electrochem. Soc.* **1997**, *144*, 55.

(52) Jennings, G. K.; Yong, T.-H.; Munro, J. C.; Laibinis, P. E. *J. Am. Chem. Soc.* **2003**, *125*, 2950.

(53) Azzaroni, O.; Cipollone, M.; Vela, M. E.; Salvarezza, R. C. *Langmuir* **2001**, *17*, 1483.

(54) Jennings, G. K.; Munro, J. C.; Laibinis, P. E. *Adv. Mater.* **1999**, *11*, 1000.

(55) Azzaroni, O.; Schilardi, P. L.; Salvarezza, R. C. *Appl. Phys. Lett.* **2002**, *80*, 106156.

(56) Azzaroni, O.; Schilardi, P. L.; Salvarezza, R. C. In *Encyclopedia of Nanoscience and Nanotechnology*; Nalwa, H., Ed.; American Scientific Publishers: Stevenson Ranch, CA, 2003.

(57) Scherer, J.; Vogt, M. R.; Magnussen, O.; Behm, R. J. *Langmuir* **1997**, *13*, 7045.

(58) Kondo, T.; Sumi, T.; Uosaki, K. *J. Electroanal. Chem.* **2002**, *538−539*, 59.

(59) Weisshaar, D. E.; Lamp, B. D.; Porter, M. D. *J. Am. Chem. Soc.* **1992**, *114*, 5860.

(60) Azzaroni, O.; Vela, M. E.; Andreasen, G.; Carro, P.; Salvarezza, R. C. *J. Phys. Chem. B* **2002**, *106*, 12267.

(61) Sellers, H.; Ulman, A.; Shnidman, Y.; Eilers, J. E. *J. Am. Chem. Soc*. **1993**, *115*, 9389.

(62) Yourdshahyan, Y.; Rappe, A. M. *J. Chem. Phys.* **2002**, *117*, 825.

(63) Beardmore, K. M.; Kress, J. D.; Gronbech-Jensen, N.; Bishop, A. R. *Chem. Phys. Lett.* **1998**, *286*, 40.

(64) Akinaga, Y.; Najajima, T.; Hirao, K. *J. Chem. Phys.* **2001**, *114*, 8555.

(65) Gottschalck, J.; Hammer, B. *J. Chem. Phys.* **2002**, *116*, 784.

(66) Becke, A. D. *J. Chem. Phys.* **1993** , *98*, 5648.

(67) Hay, P.; Wadt, R. *J. Chem. Phys.* **1985**, *82,* 299.

(68) Levine, I. N. *Quantum Chemistry*, 5th ed.; Prentice Hall: Upper Saddle River, NJ, 2000; p 492.

(69) Frisch, M. J.; Trucks, G. W.; Schlegel, H. B.; Scuseria, G. E.; Robb, M. A.; Cheeseman, J. R.; Zakrzewski, V. G.; Montgomery, J. A., Jr.; Stratmann, R. E.; Burant, J. C.; Dapprich, S.; Millam, J. M.; Daniels, A. D.; Kudin, K. N.; Strain, M. C.; Farkas, O.; Tomasi, J.; Barone, V.; Cossi, M.; Cammi, R.; Mennucci, B.; Pomelli, C.; Adamo, C.; Clifford, S.; Ochterski, J.; Petersson, G. A.; Ayala, P. Y.; Cui, Q.; Morokuma, K.; Malick, D. K.; Rabuck, A. D.; Raghavachari, K.; Foresman, J. B.; Cioslowski, J.; Ortiz, J. V.; Stefanov, B. B.; Liu, G.; Liashenko, A.; Piskorz, P.; Komaromi, I.; Gomperts, R.; Martin, R. L.; Fox, D. J.; Keith, T.; Al-Laham, M. A.; Peng, C. Y.; Nanayakkara, A.; Gonzalez, C.; Challacombe, M.; Gill, P. M. W.; Johnson, B. G.; Chen, W.; Wong, M. W.; Andres, J. L.; Head-Gordon, M.; Replogle, E. S.; Pople, J. A. *Gaussian 98*; Gaussian, Inc.: Pittsburgh, PA, 1998.

(70) Ferral, A.; Paredes-Olivera, P.; Macagno, V.; Patrito, E. M. *Surf. Sci.* **2003**, *525*, 85.

(71) Bensebaa, F.; Zhou Y.; Deslandes, Y.; Kruus, E.; Ellis, T. H. *Surf. Sci.* **1998**, *405*, L472.

(72) Chong, D. P.; Gritsenko, O. V.; Baerends. E. J. *J. Chem. Phys.* **2002**, *116*, 1760.

(73) Sellers, H.; Patrito, E. M.; Paredes Olivera, P. *Surf. Sci.* **1996**, *356*, 222.

(74) Crispin, X.; Geskin, V. M.; Bureau, C.; Lazzaroni, R.; Schmickler, W.; Brédas, J. L. *J. Chem. Phys.* **2001**, *115*, 10493.

(75) Sexton, B. A, Hughes, A. E. *Surf. Sci*. **1984**, *140*, 227.

(76) Kuznetsov, A.; Maslii, A. N.; Shapnik, M. S. *Russ. J. Electrochem*. **2000**, *36*, 1309.

(77) Kondoh, H.; Iwasaki, M.; Shimada, T.; Amemiya, K.; Yokoyama, T.; Ohta, T.; Shimomura, M.; Kono, S. *Phys. Rev. Lett.* **2003**, *90*, 066102-1

(78) Halley, J. W.; Walbran, S. In *Interfacial Electrochemistry*; Wieckowski, A., Ed.; Marcel Dekker Inc.: New York, 1999; p 9.

(79) Pirug, G.; Bonzel, H. P. In *Interfacial Electrochemistry*; Wieckowski, A., Ed.; Marcel Dekker Inc.: New York, 1999; p 270.

(80) Kakiuchi, T.; Usui, H.; Hobara, D.; Yamamoto, M. *Langmuir* **2002**, *18*, 5231.

(81) Hobara, D.; Miyake, K.; Imabayashi, S.; Niki, K.; Kakiuchi, T. *Langmuir* **1998**, *14*, 3590.